A Low-Voltage Ride-Through Strategy Using Mixed Potential Function for Three-Phase Grid-Connected PV Systems

Hao Wen, Meghdad Fazeli

Electrical and Electronic Engineering Department, Swansea University, UK

Abstract

This paper presents a new control strategy for low-voltage ride-through for 3-phase grid-connected photovoltaic systems. The proposed fault ride through control algorithm, which is designed based on mixed potential function, can protect the inverter from overcurrent failure under both symmetric and asymmetric faults, reduce the double frequency oscillation and provides reactive power support by applying a voltage compensation unit. With the proposed method, the inverter can also inject sinusoidal current during asymmetric faults. The method does not require a hard switch to switch from the Maximum Power Point Tracking (MPPT) to a non-MPPT algorithm, which ensures a smooth transition.

Keywords: Current Control, fault-ride-through, photovoltaic, micro-grids, large-signal analysis.

1. Introduction

During the last decades, the use of distributed energy resources (DERs) has increased due to economic, technical and environmental concerns [1], [2]. With the rapid increase of grid-connected photovoltaic (PV) generation, PV systems should be more reliable and

*Corresponding author

Email address: 688418@swansea.ac.uk (Hao Wen)

provide high quality services, beyond the basic power delivery during grid voltage sags [3]-[8]. Power quality and current curtailment are the most important aspects of the grid-connected power converters under grid faults. Power quality issues include: injection of non-sinusoidal inverter current during unbalanced grid faults, and the existence of double grid frequency oscillation in inverter output active power and DC-link voltage. It is also crucial to prevent the activation of the inverter's overcurrent protection during both symmetric and asymmetric faults. According to the recently revised grid codes, PV systems are supposed to stay connected during grid faults [7]. Thus, when a fault occurs, the control strategy must be capable to protect the inverter from overcurrent failure for a short period of time. This is known as low-voltage ride-through (LVRT). The exact LVRT requirements (e.g. voltage sag vs time characteristic, and the required reactive power support vs voltage sag) may differ from one country to the other. For example, Fig.1 illustrates the Chinese regulation of voltage sag vs its duration [9]. As it can be seen, even when voltage drops to 0 pu, the PV system must remain connected for 0.15s. Furthermore, a certain amount of reactive power needs to be injected to support the grid when the fault occurs [8], which will be discussed later.

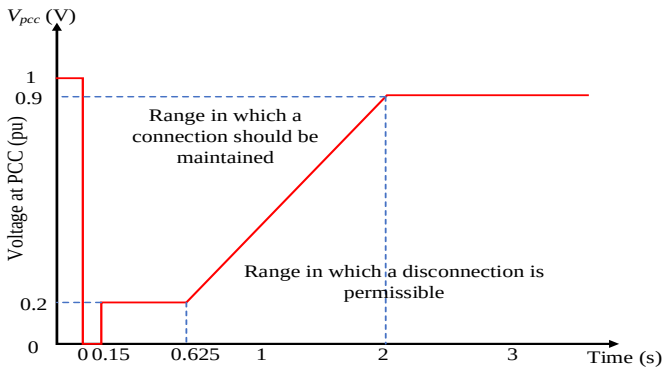

Figure 1: LVRT requirements in China [9].

Another issue is that during asymmetric faults, active power and DC-link voltage contain double grid frequency oscillation. This phenomenon has a negative impact on the life

cycle of the DC-link capacitor [7]. Also, during asymmetric faults, the inverter may inject non-sinusoidal current to the grid. Therefore, an LVRT control method (for a grid-connected PV system under different types of faults) should:

1) prevent overcurrent failure (current curtailment);
2) reduce the double grid frequency oscillation for both active power and DC-link voltage;
3) control the DC-link voltage;
4) control the inverter current properly (i.e. injecting sinusoidal current) during faults;
5) inject a certain amount of reactive power.

Different methods have been considered in the literature. E.g., in [8] a control strategy for limiting the inverter current in islanded mode is studied. However, the inverter in [8] is connected to a constant DC-voltage source which is not a precise representation of a renewable system. Obviously, the dynamics of the PV system, including the Maximum Power Point Tracking (MPPT) algorithm, the DC-link voltage control and the current loop controller can affect the operation of the entire system. E.g. while the LVRT must not disturb the MPPT during normal operation, it should limit the input power during faults and provide a smooth transition between the two modes. Moreover, in [8], the current is limited to double rated value during both symmetric and asymmetric faults, which seems to be too high, especially for asymmetric faults where voltage sags are relatively smaller. Similarly, [10] proposes an LVRT control scheme using symmetrical components in the synchronous frame for grid-connected inverter without considering a renewable energy source, neither a PV nor a wind turbine. In [11], an instantaneous active power controller is presented, which results in non-sinusoidal inverter currents under asymmetric faults. Thus, the load will consume more power (both active and reactive) during faults. Consequently, the consumer will have to pay more for the electricity. In [12], a control strategy

is proposed using symmetrical components, however, the injected active power contains significant double frequency oscillation. Ref. [7] proposes an LVRT algorithm for a two-stage 3-phase grid-connected PV system, where a hard switch is needed to move from MPPT mode to non-MPPT mode after detecting the fault. This can lead to a non-smooth transition between the two modes. Moreover, [7] only investigates asymmetric faults. In summary, unlike previous arts, this paper proposes a comprehensive LVRT algorithm, which can be used for both symmetric and asymmetric faults in a low voltage distribution network with PV system directly connected to the grid. Furthermore, the proposed method does not require a hard switch to switch from MPPT to a non-MPPT algorithm, which ensures a smooth transition. Also, a reactive power injection block is proposed to support the grid under faults. Considering the above, the proposed LVRT control strategy can:

1) operate for both symmetric and asymmetric faults;
2) prevent activation of overcurrent protection through limiting the inverter current to 1.5 pu during symmetric faults and 1 pu during asymmetric faults;
3) provide high quality sinusoidal inverter voltage and current during faults;
4) reduce the double grid frequency oscillation;
5) eliminate the need to switch from MPPT mode to non-MPPT mode;
6) support voltage through reactive power injection.

To achieve the above objectives, a voltage compensation unit (VCU) is proposed, which uses the mixed potential function to determine how much PV power should reduce for a voltage drop in order to comply with the Lyapunov criterion. This method will be validated through simulations.

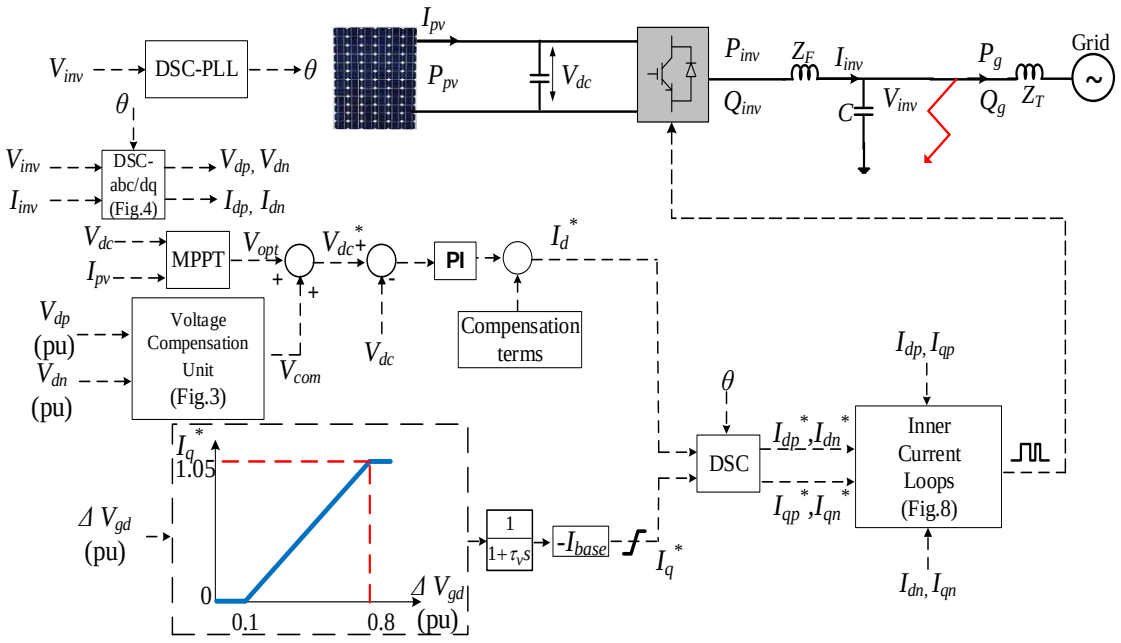

Figure 2: The system understudy plus the proposed control scheme for grid-connected PV.

The paper is structured as follow: in Section II, the proposed LVRT control scheme is presented, including the method to estimate the positive sequence and negative sequence components for voltage and current in the synchronous frame, voltage loop design with the proposed current limiting strategy, reactive power injection and current loop design. The proposed control strategy is verified by MATLAB/Simulink simulations in Section III. Finally, conclusions are drowned at the end to summarize the advantage of the proposed method in Section IV.

2. Proposed Control Strategy

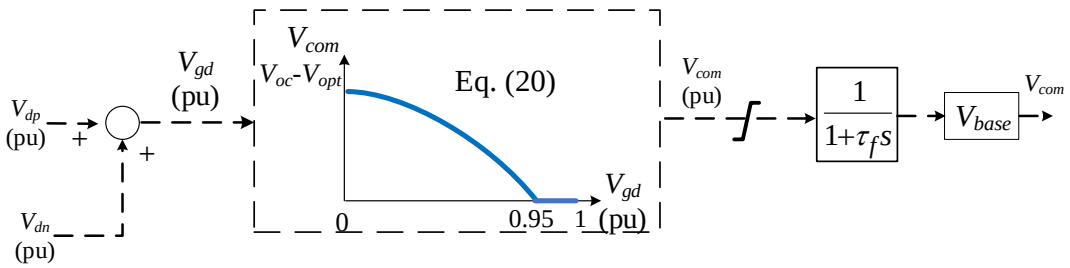

Figure 3: Structure of the proposed voltage compensation unit.

The understudy system with the proposed LVRT strategy is illustrated in Fig. 2. A conventional P&O MPPT algorithm is used. The Delayed Signal Cancellation (DSC) method, explained in [13], [14], is used to separate the symmetrical components for both inverter-/grid-side voltage and current. A DSC-based PLL, which is explained in [15], synchronizes the PV system with the grid. The proposed control strategy, which uses the classic cascaded voltage and current loops in dq-frame, includes a VCU unit (detailed in Fig. 3). The current loop consists of four PI controllers for dq-currents in positive (I_{dp}, I_{qp}) and negative (I_{dn}, I_{qn}) sequences. A reactive power injection block is proposed, which determines how much reactive power should be injected during faults according to the Chinese regulation. The proposed scheme is detailed below:

2.1 Symmetrical Components Generation

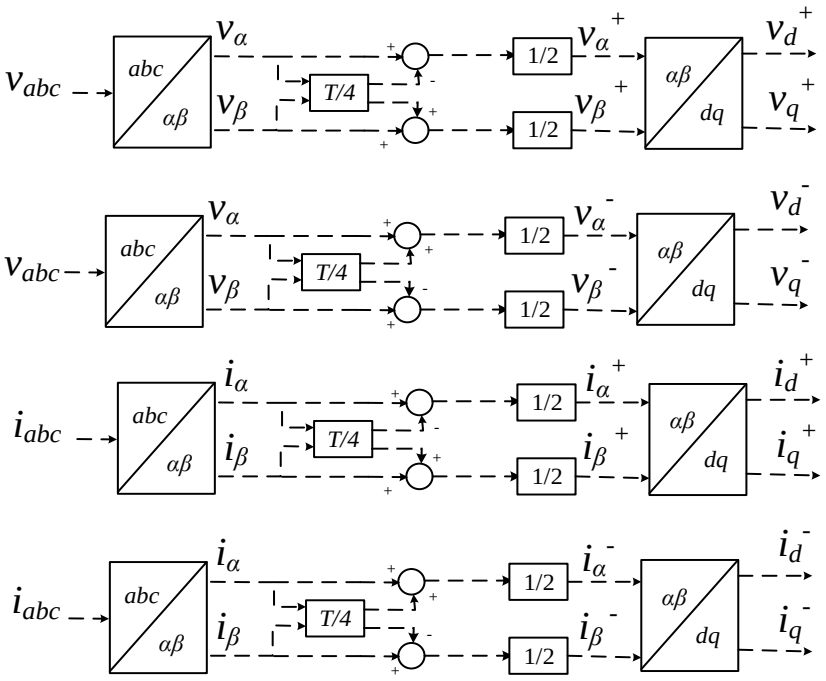

Figure 4: The diagram of the DSC method.

In this paper, the well-known method of DSC is used for sequence component separation. As shown in Fig. 4, the DSC method can be written as [14]:

$$v_{p(\alpha,\beta)} = \frac{1}{2}\left[v_{\alpha,\beta}(t) + jv_{\alpha,\beta}(t - \frac{T}{4}) \right]$$
$$v_{n(\alpha,\beta)} = \frac{1}{2}\left[v_{\alpha,\beta}(t) - jv_{\alpha,\beta}(t - \frac{T}{4}) \right] \quad (1)$$

where $V_{p(\alpha, \beta)}$ and $V_{n(\alpha, \beta)}$ are the estimations of the positive and negative sequence signals in stationary frame, and T is the signal period, which is the same as the grid period. The symmetrical components for current can be estimated using (1) as well. Then both voltage and current signals are converted to the synchronous (dq) frame using the standard Park Transform. Obviously, during normal operation and under symmetric faults, there are no negative sequence components. However, during asymmetric faults, the negative sequence components appear in both voltage and current, which leads to the voltage and current oscillation. As a result, the classic two-channel dq current loops are not reliable. By separating the negative sequence components from the positive consequence components, a four-channel current loop structure (see Fig. 8) can be used to alleviate the issue. From the basic theory of symmetrical sequence components, ($v=v_p+v_n+v_0$), it is possible to claim that all the voltage and current signals used in the next section are the sum of the positive and negative sequence components.

2.2 Voltage Compensation Unit

Resembling the PV system to a synchronous generator, one can argue that the PV array input power P_{pv} resembles the input mechanical power. In a synchronous generator, the mechanical power is assumed constant after a fault since it cannot be changed very quickly. This divides the power vs power angle characteristic (see Fig. 5) into accelerating (red shadow A_1) and maximum decelerating (red shadow A_2) areas.

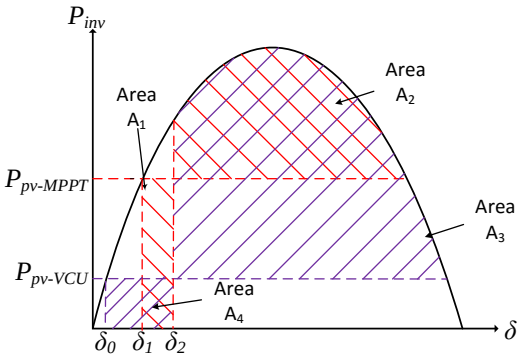

Figure 5: Inverter Power vs power angle characteristic.

According to equal area criteria [16], the system remains stable if $A_1 \leq A_2$. As illustrated in Fig. 5, in a PV system, reducing P_{pv} after a fault (i.e. from $P_{pv\text{-}MPPT}$ to $P_{pv\text{-}VCU}$) reduces the accelerating area (purple shadow A_4) and increases the maximum decelerating area (purple shadow A_3), which in turns increases the stability margin. Therefore, the proposed VCU, shown in Figs. 2 and 3, is designed to reduce the generated power after a fault.

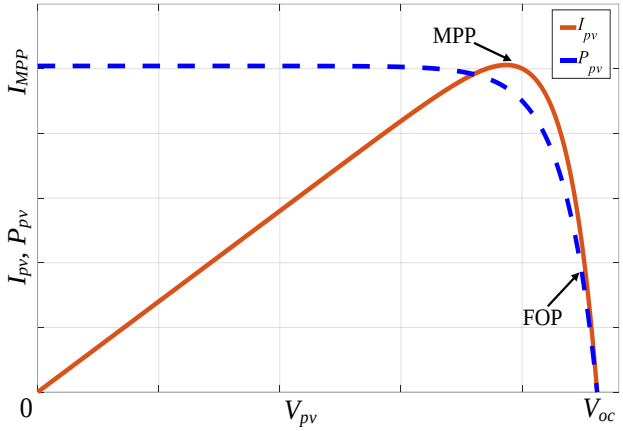

Figure 6: P_{pv}-V_{pv} & I_{pv}-V_{pv} characteristic curves.

As it can be seen from the P_{pv}-V_{pv} characteristic in Fig. 6, it is possible to reduce P_{pv} through either adding the compensation voltage V_{com} (from the VCU) to the optimum voltage V_{opt} (from the MPPT algorithm) or subtracting V_{com} from V_{opt}. However, considering the I_{pv}-V_{pv} curve (the dashed blue line), it can be found that only when the PV is operating at the right-hand side of the MPP (e.g. the fault operation point (FOP)), the

output current of the PV can be reduced. Thus, as illustrated in Fig. 2, the VCU determines the reference DC-link voltage V_{dc}^{*} through adding V_{com} to V_{opt}. By doing this, both the inverter current and power will be reduced under symmetric and asymmetric faults and there is also no need to switch the PV system from MPPT mode to a non-MPPT mode. Obviously, as the voltage sag increases, V_{com} should also increase to reduce the PV output current. Thus, this paper proposes to increase V_{com} as V_{gd} reduces where V_{gd} is the d-component of the grid voltage. As illustrated in Fig. 3, when V_{gd} becomes less than 0.95 pu (0.95, which is chosen to avoid disturbing normal operation, can change according to different standards), V_{com} gradually increases. Moreover, the VCU is designed to reduce the active power and DC-link voltage double grid frequency oscillation and to keep the inverter current sinusoidal during asymmetric faults. To do this, this paper uses the mixed potential function to define the variation of V_{com} vs V_{gd}. The mixed potential function, which first stated in Brayton-Moser's mixed potential theory [17], [18], can be used to describe the dynamics of a large class of nonlinear RLC network with two-terminal elements to investigate the stability of the network's equilibrium point, and to describe the noise of the network (here the noise is the double grid frequency oscillation of the active power and the DC-link voltage, and the non-sinusoidal inverter current) [17]-[19].

The mixed potential function P is constructed from the resistors, capacitors and inductors in the nonlinear network. According to the mixed-potential theory, if v_μ and i_μ denote the voltage and current of all the non-energy storage elements of the system and v_σ and i_σ denote the voltage and current of all capacitors of the system, the potential function P can be written as (2):

$$P(i,v) = \sum \int v_\mu di_\mu + \sum i_\sigma v_\sigma \tag{2}$$

where the first term on the right-hand side of the equal mark represents the current potential of all the non-energy storage elements, and the second term is the sum of the capacitors' energy [20]. Since the proposed system is a nonlinear dynamic model under fault conditions, the mixed-potential function can be used to describe the system [21].

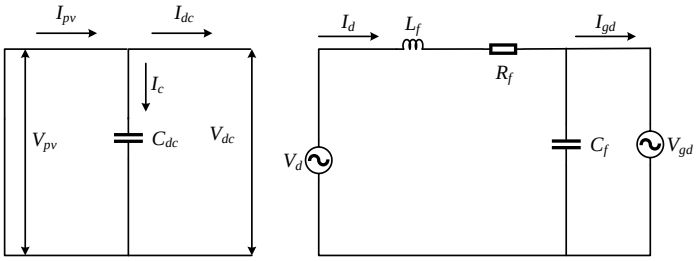

Figure 7: The simplified model of the proposed PV system.

Figure 7 shows the simplified model of a grid-connected PV system while the inverter is represented by V_d on the AC-side, and by C_{dc} on the DC-side. As mentioned above, all of the d-components are the sum of the positive and negative sequence components. The mixed potential function for the proposed model can be written as (3):

$$P(i,v) = \int_0^{i_{pv}} v_{pv} di_{pv} - i_c v_{pv} - \int_0^{i_{dc}} v_{dc} di_{dc} + \int_0^{i_d} v_d di_d - \int_0^{i_d} i_d R_f di_d - \int_0^{i_{gd}} v_{gd} di_{gd} - \left(i_d - i_{gd}\right) v_{gd} \quad (3)$$

In steady state (neglecting the losses):

$$P_g = \frac{3}{2} V_{gd} I_{gd} = V_{pv} I_{pv} = P_{pv} \quad (4)$$

where P_g is the grid active power, V_{gd} and I_{gd} are the voltage and current after the LC filter. Since the capacitor voltage is constant at steady state, I_{pv} should be equal to I_{dc}. Considering $V_{pv} = V_{dc}$, $I_{pv} = I_{dc}$, where I_c is a small value. Thus, (3) can be rewritten as (5):

$$P(i,v) = -i_c v_{pv} + \int_0^{i_d} v_d di_d - \int_0^{i_d} i_d R_f di_d - \int_0^{i_{gd}} \frac{2p_g}{3i_{gd}} di_{gd} - \left(i_d - \frac{2p_g}{3v_{gd}} \right) v_{gd} \quad (5)$$

where the first term on the right hand of the equal mark represents the DC-link capacitor's energy, the second term is the current potential of the inverter output voltage, the third

term is the current potential of the filter resistor, the fourth term is the current potential of the grid side voltage, and the last term is the filter capacitor's energy.

Since the grid side voltage V_{gd} is not a single-valued function of the grid side current I_{gd}, one can write (6):

$$\int_0^{i_{gd}} \frac{2p_g}{3i_{gd}} di_{gd} = \frac{2p_g}{3i_{gd}} I_{gd} - \int_0^{v_{gd}} \frac{2p_g}{3v_{gd}} dv_{gd} \tag{6}$$

Substituting (6) into (5), gives:

$$P(i,v) = v_d i_d - \frac{1}{2} R_f i_d^2 + \int_0^{v_{gd}} \frac{2p_g}{3v_{gd}} dv_{gd} - i_d v_{gd} - i_c v_{pv} \tag{7}$$

Equation (7) is the mixed-potential function of the proposed model. To verify whether (7) is the correct mixed-potential function, the partial derivatives of (7) must comply with (8) [18]-[20]:

$$\begin{aligned} \frac{\partial p}{\partial v_\sigma} &= -C \frac{dv_\sigma}{dt} \\ \frac{\partial p}{\partial i_\mu} &= L \frac{di_\mu}{dt} \end{aligned} \tag{8}$$

Equation (8) is the only criterion to verify the validity of the mixed-potential function. Using (7), the following differential equations of the proposed model can be obtained:

$$\begin{aligned} \frac{\partial p}{\partial v_{pv}} &= -i_c = -C_{dc} \frac{dv_{pv}}{dt} \\ \frac{\partial p}{\partial v_{gd}} &= \frac{2p_g}{3v_{gd}} - i_d = -\left(i_d - i_{gd}\right) = -C_f \frac{dv_{gd}}{dt} \\ \frac{\partial p}{\partial I_d} &= v_d - R_f i_d - v_{gd} = L_f \frac{di_d}{dt} \end{aligned} \tag{9}$$

As noted, (9) is in accordance with (8), and consequently, (7) corresponds to the system state equations and it is the correct mixed-potential function of the system. In general, the unified form of P is given as (10) [18]-[20]:

$$P(i,v) = -A(i) + B(v) + (i, \gamma v - \alpha) \tag{10}$$

Thus, in this model, $P(i, v)$ can be written as (11):

$$P(i,v) = -\frac{1}{2} R_f i_d^2 + \int_0^{V_{gd}} \frac{2p_g}{3v_{gd}} dv_{gd} + \begin{pmatrix} i_c & i_d \end{pmatrix} \times \left(\begin{pmatrix} -1 & 0 \\ 0 & -1 \end{pmatrix} \begin{pmatrix} v_{pv} \\ v_{gd} \end{pmatrix} - \begin{pmatrix} 0 \\ -v_d \end{pmatrix} \right) \tag{11}$$

The proposed method is to use the mixed potential function to determine for a certain V_{gd} drop, how much P_{pv} should be reduced (i.e. P_{pv}=Fcn(V_{gd})) to comply with the Lyapunov criterion. One can define μ_1 and μ_2 as the minimum eigenvalue of the matrices $L^{-1/2} A_{ii}(i) L^{-1/2}$ and $C^{-1/2} B_{vv}(v) C^{-1/2}$, respectively, where, $A_{ii}(i)$ and $B_{vv}(v)$ are the second-order partial derivative of $A(i)$ and $B(v)$. According to the fifth theorem of the mixed-potential theory [17] and Lyapunov criterion [22], if for all i and v:

$$\mu_1 + \mu_2 > 0 \text{ and } P(i,v) \to \infty, as \left|i\right| + \left|v\right| \to \infty \tag{12}$$

then all the solutions of (9) approach the equilibrium point, which means the oscillation is minimized [21]. To calculate μ_1 and μ_2, $A_{ii}(i)$ and $B_{vv}(v)$ are calculated first:

From (11), $A(i)$ and $B(v)$ can be written as:

$$\begin{aligned} A(i) &= \frac{1}{2} R_f i_d^2 \\ B(v) &= \int_0^{p_{gd}} \frac{2p_g}{3v_{gd}} dv_{gd} \end{aligned} \tag{13}$$

Then from (13), $A_{ii}(i)$ and $B_{vv}(v)$ can be written as (14):

$$\begin{aligned} A_{ii}(i) &= \frac{\partial^2 A(i)}{\partial i^2} = R_f \\ B_{vv}(v) &= \frac{\partial^2 B(v)}{\partial v^2} = -\frac{2p_g}{3v_{gd}^2} \end{aligned} \tag{14}$$

Thus, μ_1 and μ_2 can be derived:

$$\begin{aligned} \mu_1 &= \frac{R_f}{L} \\ \mu_2 &= -\frac{2P_g}{3CV_{gd}^2} \end{aligned} \tag{15}$$

Since the proposed model is grid-connected, P_g=P_{pv} (neglecting the losses). Equation (12) can be re-written as:

$$\mu_1 + \mu_2 = \frac{R_f}{L_f} - \frac{2P_{pv}}{3C_{dc}V_{gd}^2} > 0 \tag{16}$$

Thus, the Lyapunov criterion of the proposed model is (16). From this criterion, the variation of P_{pv} vs V_{gd} can be derived:

$$P_{pv} < \frac{3R_f C_{dc}}{2L_f} V_{gd}^2 \tag{17}$$

where, V_{gd} is the grid voltage, which will drop when a fault occurs. Equation (17) approximately determines the maximum P_{pv} for a V_{gd} such that system complies with the Lyapunov criterion. Equation (17) will be used to define the relationship between V_{com} and V_{gd} in the proposed VCU:

Using (17) for V_{gd} = 0:0.1:1 pu (i.e. for 0.1 pu steps of V_{gd}), $P_{pv\text{-}limit}$ is calculated:

$$P_{pv-limit} = \frac{3R_f C_{dc}}{2L_f} V_{gd}^2 \tag{18}$$

Obviously, P_{pv}< $P_{pv\text{-}limit}$ in order to comply with Lyapunov criterion. Then, the calculated $P_{pv\text{-}limit}$ (for each V_{gd}) is used in (the right-hand side of) the P_{pv} vs V_{pv} characteristic (see Fig. 6) to get the desirable V_{com}. Doing this for each 0.1 pu step of V_{gd}, and using the MATLAB 'polyfit' function (for the calculated V_{com} vs V_{gd} points), (19) can be formed:

$$V_{com} = k_m(aV_{gd}^5 + bV_{gd}^4 + cV_{gd}^3 + dV_{gd}^2 + eV_{gd} + f) \tag{19}$$

where, k_m is a safety margin coefficient (e.g. k_m=1.05) to make sure that the P_{pv} associated with the calculated V_{com} from 19) complies with (17) i.e. is less than $P_{pv\text{-}limit}$. A hard limit of V_{limit}=V_{oc} -$V_{opt\text{-}max}$, where V_{oc} is the open circuit voltage of the PV array and $V_{opt\text{-}max}$ is the optimum voltage from the MPPT at 1 pu solar irradiation, is applied to make sure that V_{com} will not become more than V_{oc}. Note that with the solar irradiation varies, both V_{oc}

and V_{opt} varies almost proportionally, thus V_{limit} can be a fixed value. The calculated V_{com} is added to V_{opt} to get V_{dc}^*. Then a classic PI controller (Fig. 2) is used for the voltage loop to determine I_d^*, which is the reference d-component current.

2.3 Current loop

As illustrated in Fig. 8, the current loop consists of four classic PI controllers for positive and negative sequences of d- and q-components. The modulating signal m is calculated through adding the positive and negative modulating signals $m=m_p+m_n$, while m_p and m_n are calculated by using the inverse Park transform. It is noted that the phase angle used in the negative channel is $-\theta$.

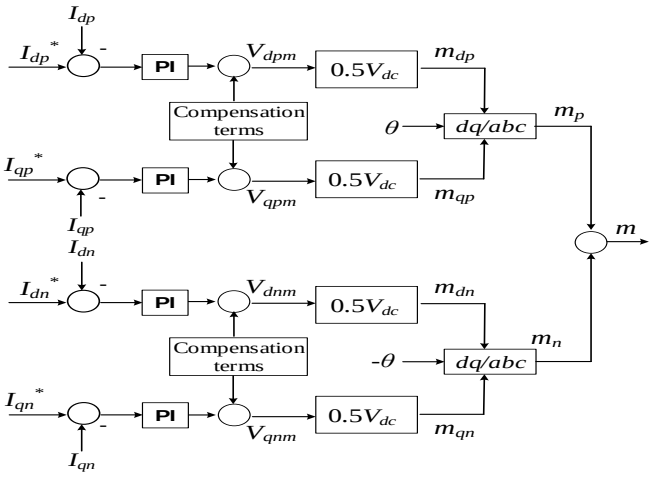

Figure 8: Current Loop.

The integral gain of the PI controllers is designed using the characteristic equation:

$$s^2 + (\frac{R_f + K_p}{L_f})s + \frac{K_i}{L_f} = 0 \tag{20}$$

In (20), R_f and L_f are the LC filter resistance and inductance. Assuming the bandwidth to be ω_n rad/s, the integral gain $K_i = L_f\omega_n^2$. K_p will be designed to make the controller robust against grid disturbances. Using characteristic equation, for a critically damped system, $K_p=2L_f\omega_n-R_f$. In order to improve the controller robustness, it is possible to choose a $K_p>2L_f\omega_n-R_f$, provided that it does not violate the system stability [23]. To investigate the

effect of K_p on the system root locus, one can re-write the characteristic equation of (20) as follow:

$$s^2 + \frac{R_f}{L_f}s + \frac{K_i}{L_f} + \frac{K_p}{L_f}s = 0 \tag{21}$$

$$1 = \frac{-\frac{K_p}{L_f}s}{s^2 + \frac{R_f}{L_f}s + \frac{K_i}{L_f}} \tag{22}$$

$$1 + \frac{\frac{K_p}{L_f}s}{s^2 + \frac{R_f}{L_f}s + \frac{K_i}{L_f}} = 0 \tag{23}$$

Equation (23) is basically the characteristic equation, thus, from the definition of characteristic equation, the equivalent Open-Loop Transfer Function (OLTF) for the control plant, which contains K_p, can be written as (24):

$$OPLF = \frac{\frac{K_p}{L_f}s}{s^2 + \frac{R_f}{L_f}s + \frac{K_i}{L_f}} \tag{24}$$

where, $K_i = L_f\omega_n^2$. Using (24), the root locus chart can be drawn for K_p variations. This method will be used in the simulation section to design the current loops.

2.4 Reactive Power Injection

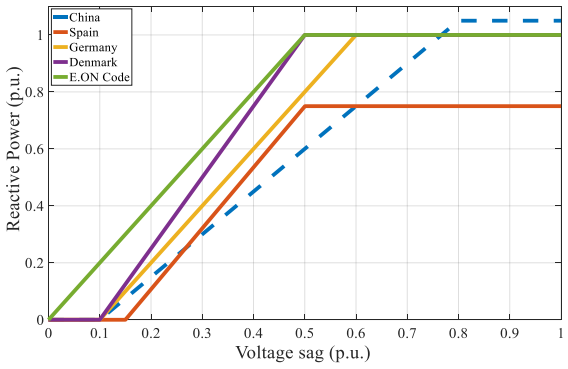

Figure 9: Grid Standards for reactive power injection of each country [7].

Figure 9 illustrates how much reactive power should be injected with respect to the voltage sags in different countries [7]. According to [24], a PV plant must be capable of controlling the reactive power supplied by the PV power plant. Since the DSC-PLL keeps the positive sequence of V_{inv} q-component $V_{qp}\approx 0$ (at steady state) and the negative sequence V_{qn} is too small when the fault appears, this paper proposes using ΔV_{gd} (ΔV_{gd}=1-V_{gd}) for reactive power regulation. This paper uses the Chinese standard (the dashed blue curve in Fig. 9) such that for ΔV_{gd}<0.1 pu; I_q^*=0, for ΔV_{gd} >0.8 pu; I_q^*=1.05 pu, and for 0.1< ΔV_{gd} <0.8 pu; I_q^* varies linearly.

3. Simulation Results

3.1 System Parameters

In this section, the system shown in Fig. 2 (which includes the proposed control strategy) is simulated in MATLAB/SIMULINK environment. The grid frequency is f=50Hz. The rest of the parameters are shown in the table 1. Note that all results are presented in per unit (pu) value.

Table 1. System's parameters

Variable	Value
Line to Line voltage $V_{L\text{-}L}$	650 V
DC link capacitor C_{dc}	210 μF
LC filter parameters	R_f=0.2 Ω L_f =3 mH
Line Impedance	R_l=*0.38* Ω L_l=*0.15* mH
Current Loop PI controller	K_p=24 K_i=1598.7

Using the data provided in Table 1, (17) for the simulated system is:

$$P_{pv} < 0.021V_{gd}^2$$

Considering k_m=1.05, (19) for the simulated system is:

$$V_{com} = -3.6771V_{gd}^5 + 7.0739V_{gd}^4 - 4.6767V_{gd}^3 + 1.5089V_{gd}^2 - 0.5786V_{gd} + 0.3496$$

Choosing ω_n= 730 rad/s (f_n=116 Hz), the integral gain $K_i=L_f\omega_n^2$= 1598.7. As it can be seen from Fig. 10, which depicts the current loop root locus for the simulated system using (24), by choosing K_p=24 the system remains stable and provides a good robustness.

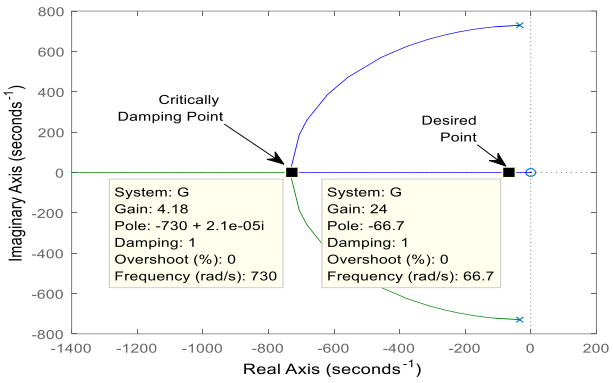

Figure 10: Root locus diagram of the proposed current loop.

The following test scenarios are simulated:

3.2 Double Line Fault and Double Line to Ground Fault

During normal operation, P_{pv}, which is the power generates by the PV array, is 1pu. It is assumed that the PV system does not contribute any reactive power during normal operation. It is known that the double grid frequency oscillation only appears under asymmetric faults. To verify the effectiveness of the proposed VCU, a double line (DL) fault will occur (see Fig. 2) at t=1 s and last for 0.2 s. The following two scenarios are being compared: First, the system will be simulated with no LVRT strategy (Fig. 11). Second, the system will be simulated with the proposed LVRT strategy (Fig. 12).

When there is no LVRT strategy (Fig.11), the double grid frequency oscillation exists in both grid active power P_{inv} and DC-link voltage V_{dc}. In addition, the inverter current I_{inv} is not sinusoidal during the fault. However, when the LVRT strategy is applied (Fig. 12), P_{inv} and V_{dc} fluctuations are significantly reduced. Meanwhile, I_{inv} becomes sinusoidal during the fault. Moreover, the peak value of I_{inv} without the LVRT strategy (Fig. 11) hits the 2 pu hard limit during the whole fault period. However, I_{inv} is curtailed to less

than 1pu with the proposed LVRT strategy (Fig. 12), which ensures that the inverter over-current protection will not be activated during the fault (note that I_{inv} hits the hard limit for less than a cycle, which will not activate the overcurrent protection). It should be noticed that the reactive power is injected (in accordance with the Chinese Code) during the fault to support the grid.

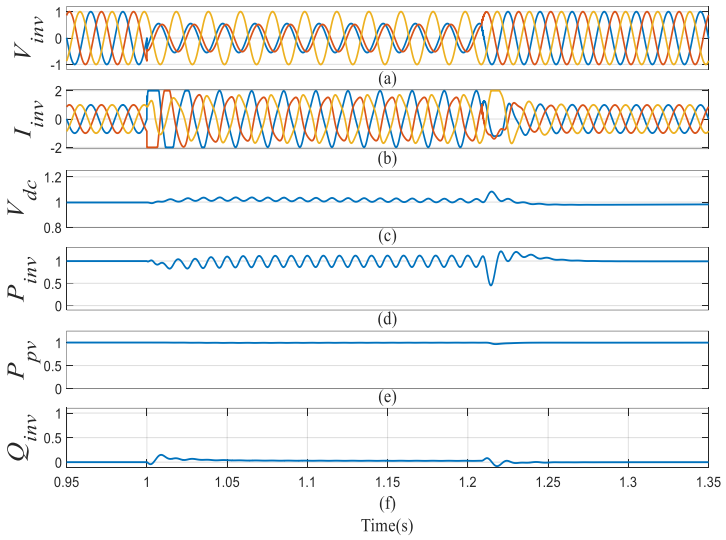

Figure 11: Simulation results under DL fault without LVRT (all in pu): (a) inverter voltage, (b) inverter current, (c) DC-link voltage, (d) inverter side active power, (e) PV power, (f) reactive power.

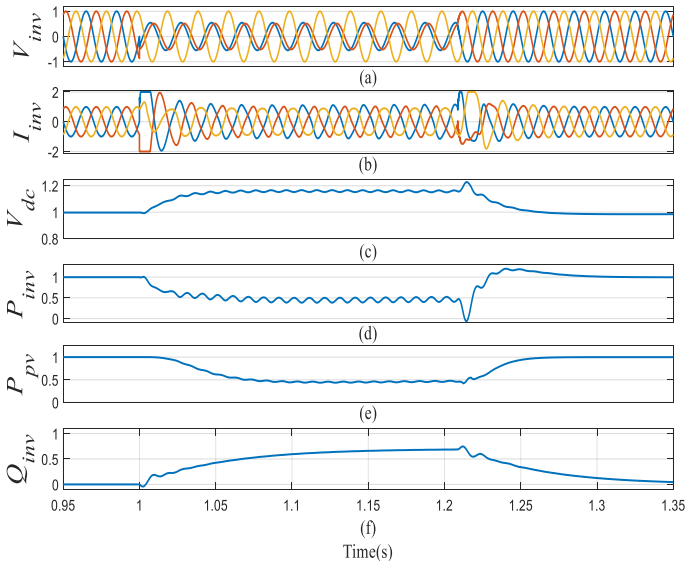

Figure 12: Simulation results under DL fault with the proposed LVRT (all in pu): (a) inverter voltage, (b) inverter current, (c) DC-link voltage, (d) inverter side active power, (e) PV power, (f) reactive power.

Since double line to ground (DLG) fault and single line to ground (SLG) fault are also asymmetric faults, the performances of the double grid frequency oscillation and inverter current without the proposed LVRT is similar to those of the DL fault. Therefore, in the following results, only the simulation with the proposed LVRT is presented.

Similarly, during DLG fault, which is shown in Fig. 13, the double grid frequency oscillation is reduced, and the inverter current is sinusoidal and limited to less than 1 pu. Since the voltage sag is deeper than a DL fault, more reactive power is injected to support the grid compared to Fig. 12.

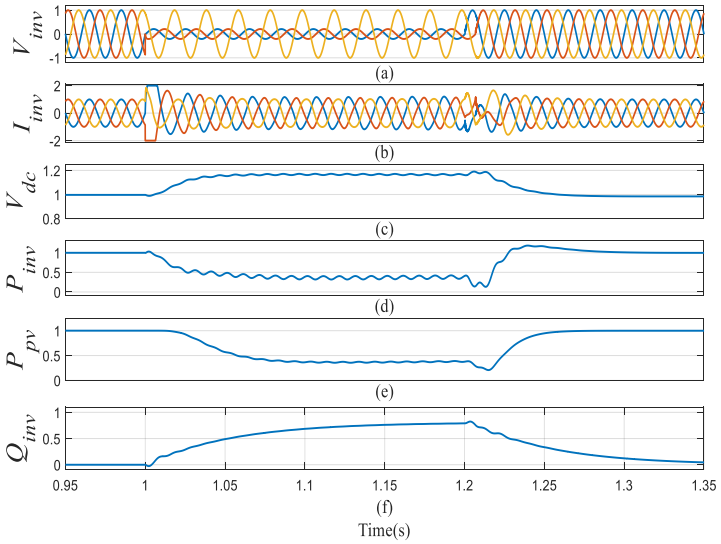

Figure 13: Simulation results under DLG fault (all in pu): (a) inverter voltage, (b) inverter current, (c) DC-link voltage, (d) inverter side active power, (e) PV power, (f) reactive power.

3.3 Single Line to Ground Fault

Figure 14 shows the simulation results for a SLG fault using the proposed LVRT strategy. Since the voltage sag is smaller than DL fault, the proposed method reduces P_{pv} less

than DL fault which results to I_{inv} limited to less than 1 pu. The normal operation is restored as soon as the fault is being cleared. Compared to the DL fault, the injected reactive power is smaller, which follows the grid standard shown in Fig. 9.

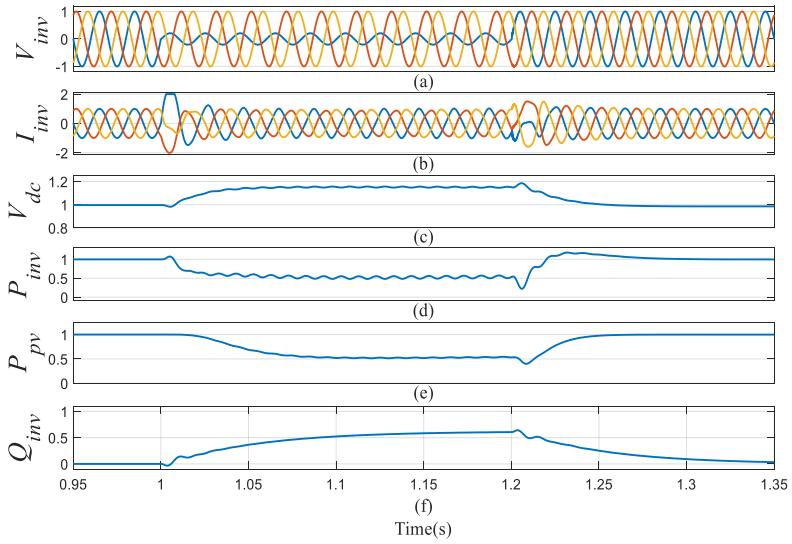

Figure 14: Simulation results under SLG fault (all in pu): (a) inverter voltage, (b) inverter current, (c) DC-link voltage, (d) inverter side active power, (e) PV power, (f) reactive power.

3.4 Three-phase fault

Figure 15 shows the result of a 3-phase fault using the proposed LVRT method. Since it is a symmetric fault, there is no double grid frequency oscillation for the inverter active power and DC-link voltage. Although I_{inv} remains pure sinusoidal even without a LVRT strategy, it will increase significantly because a 3-phase fault has the most severe voltage drop (here V_{inv} drops to less than 0.2 pu). As it can be seen from the results, to overcome the significant voltage sag, V_{dc} increases to almost V_{oc} =1.2 pu. This leads to P_{pv} and P_{inv} reduce to almost 0 pu. Thus, I_{inv} is limited to less than 1.5 pu during the fault. It should be noticed that when voltage drops to 0.2 pu, 1.05 pu reactive power is injected to the grid (in accordance with the Chinese Code), which leads to I_q^* increase. Consequently, the inverter current during 3-phase fault is more than that in other types of faults.

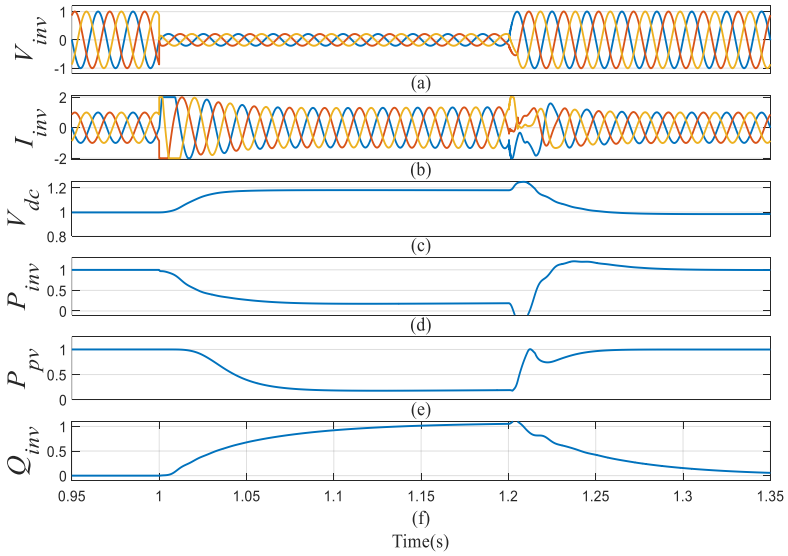

Figure 15: Simulation results under 3-phase fault (all in pu): (a) inverter voltage, (b) inverter current, (c) DC-link voltage, (d) inverter side active power, (e) PV power, (f) reactive power.

4. CONCLUSION

This paper proposes a LVRT control strategy for low voltage distribution networks with PV system directly connected to the grid. The method is based on the classic cascaded voltage and current loops in dq-frame, while the positive and negative sequence components are used to modify the reference DC-link voltage to limit the inverter current during the grid faults. The mixed-potential function is used to regulate the compensation term of the DC-link voltage. Through applying this regulation, the double grid frequency oscillation, which is appeared in inverter active power and DC-link voltage following an asymmetric fault, can be reduced. The method also generates sinusoidal inverter current during faults. The reactive power injection is used to supply the required reactive power to restore the voltage. In choosing the DC-link capacitor this should be taken into account that the proposed method increases the DC-link voltage during faults. However, since the protection systems must operate within a fracture of a second, this should not be a huge burden on an appropriate power capacitor.

The proposed method is validated in MATLAB/SIMULINK. Simulation results show the proposed LVRT control strategy can be used for both symmetric and asymmetric faults. The simulation results also demonstrate that the proposed voltage compensation unit, derived from the mixed potential function, reduces the double grid frequency oscillation. The presented results show that for a severe voltage sag (3-phase fault), the proposed method could reduce the fault current to 1.5 pu to protect the inverter from overcurrent failure. For asymmetric voltage sags, the proposed method could limit the fault current to almost rated value. In addition, this method does not require a hard switch to switch from the MPPT to a non-MPPT algorithm, which ensures a smooth transition. It is noted that the proposed method does not affect the normal operation (due to lack of space was not shown in the results).

References

[1] Olivares, D.E., Mehrizi-Sani, A., Etemadi, A.H., Cañizares, C.A., Iravani, R., Kazerani, M., Hajimiragha, A.H., Gomis-Bellmunt, O., Saeedifard, M., Palma-Behnke, R., Jiménez-Estévez, G.A., and Hatziargyriou, N.D.: 'Trends in Microgrid Control', IEEE Transactions on Smart Grid, 2014, 5, (4), pp. 1905-1919. doi: 10.1109/TSG.2013.2295514

[2]Lasseter, B.: 'Microgrids', Proc. IEEE Power Eng. Soc. Winter Meeting, 2002, 1, (Columbus, OH, USA), pp. 146-149

[3]Meyer, R., Zlotnik, A., and Mertens, A.: 'Fault ride through control of medium-voltage converters with LCL filter in distributed generation systems', (2013, edn.), pp. 1954-1961. doi: 10.1109/ECCE.2013.6646947

[4]Hu, J., He, Y., Xu, L., and Williams, B.W.: ‘Improved Control of DFIG Systems During Network Unbalance Using PIR Current Regulators’, IEEE Transactions on Industrial Electronics, 2009, 56, (2), pp. 439-451. doi: 10.1109/TIE.2008.2006952

[5]Camacho, A., Castilla, M., Miret, J., Vasquez, J.C., and Alarcon-Gallo, E.: ‘Flexible Voltage Support Control for Three-Phase Distributed Generation Inverters Under Grid Fault’, IEEE Transactions on Industrial Electronics, 2013, 60, (4), pp. 1429-1441. doi: 10.1109/TIE.2012.2185016

[6]Miret, J., Castilla, M., Camacho, A., Vicuña, L.G.d., and Matas, J.: ‘Control Scheme for Photovoltaic Three-Phase Inverters to Minimize Peak Currents During Unbalanced Grid-Voltage Sags’, IEEE Transactions on Power Electronics, 2012, 27, (10), pp. 4262-4271. doi: 10.1109/TPEL.2012.2191306

[7]Afshari, E., Moradi, G.R., Rahimi, R., Farhangi, B., Yang, Y., Blaabjerg, F., and Farhangi, S.: ‘Control Strategy for Three-Phase Grid-Connected PV Inverters Enabling Current Limitation Under Unbalanced Faults’, IEEE Transactions on Industrial Electronics, 2017, 64, (11), pp. 8908-8918. doi: 10.1109/TIE.2017.2733481

[8]Sadeghkhani, I., Golshan, M.E.H., Guerrero, J.M., and Mehrizi-Sani, A.: ‘A Current Limiting Strategy to Improve Fault Ride-Through of Inverter Interfaced Autonomous Microgrids’, IEEE Transactions on Smart Grid, 2017, 8, (5), pp. 2138-2148. doi: 10.1109/TSG.2016.2517201

[9]Jia, Y., Gao, Y., Xu, Z., Wong, K.P., Lai, L.L., Xue, Y., Dong, Z.Y., and Hill, D.J.: ‘Powering China's Sustainable Development with Renewable Energies: Current Status and Future Trend’, Electric Power Components and Systems, 2015, 43, (8-10), pp. 1193-1204. doi: https://doi.org/10.1080/15325008.2015.1009585

[10]Alepuz, S., Busquets-Monge, S., Bordonau, J., Martinez-Velasco, J.A., Silva, C.A., Pontt, J., and Rodriguez, J.: 'Control Strategies Based on Symmetrical Components for Grid-Connected Converters Under Voltage Dips', IEEE Transactions on Industrial Electronics, 2009, 56, (6), pp. 2162-2173. doi: 10.1109/TIE.2009.2017102

[11]R. Teodorescu, M.L.a.P.R.: 'Grid Converters for Photovoltaic and Wind Power Systems' (Wiley, 2011. 2011). doi: 10.1002/9780470667057

[12]Camacho, A., Castilla, M., Miret, J., Borrell, A., and de Vicuna, L.G.: 'Active and Reactive Power Strategies With Peak Current Limitation for Distributed Generation Inverters During Unbalanced Grid Faults', IEEE Transactions on Industrial Electronics, 2015, 62, (3), pp. 1515-1525. doi: 10.1109/TIE.2014.2347266

[13]Cárdenas, R., Dı´az, M., Rojas, F., and Clare, J.: 'Fast Convergence Delayed Signal Cancellation Method for Sequence Component Separation', IEEE Transactions on Power Delivery, 2015, 30, (4), pp. 2055-2057. doi: 10.1109/TPWRD.2014.2373038

[14]Svensson, J., Bongiorno, M., and Sannino, A.: 'Practical Implementation of Delayed Signal Cancellation Method for Phase-Sequence Separation', IEEE Transactions on Power Delivery, 2007, 22, (1), pp. 18-26. doi: 10.1109/TPWRD.2006.881469

[15]Qicheng, H., and Rajashekara, K.: 'An improved delayed signal cancellation PLL for fast grid synchronization under distorted and unbalanced grid condition', (2016, edn.), pp. 1-7. doi: 10.1109/IAS.2016.7731867

[16]Kundur, P., Balu, N.J., and Lauby, M.G.: 'Power system stability and control' (McGraw-Hill, 1994. 1994)

[17]Brayton, R.K., and Moser, J.K.: 'A THEORY OF NONLINEAR NETWORKS I', Quarterly of Applied Mathematics, 1964, 22, (1), pp. 1-33

[18]Brayton, R.K., and Moser, J.K.: ‘A THEORY OF NONLINEAR NETWORKS, II’, Quarterly of Applied Mathematics, 1964, 22, (2), pp. 81-104

[19]Weiss, L., Mathis, W., and Trajkovic, L.: ‘A generalization of Brayton-Moser's mixed potential function’, IEEE Transactions on Circuits and Systems I: Fundamental Theory and Applications, 1998, 45, (4), pp. 423-427. doi: 10.1109/81.669065

[20]Liu, X., Zhou, Y., Zhang, W., and Ma, S.: ‘Stability Criteria for Constant Power Loads With Multistage Filters’, IEEE Transactions on Vehicular Technology, 2011, 60, (5), pp. 2042-2049. doi: 10.1109/TVT.2011.2148133

[21]Huang, M., Peng, Y., Tse, C.K., Liu, Y., Sun, J., and Zha, X.: ‘Bifurcation and Large-Signal Stability Analysis of Three-Phase Voltage Source Converter Under Grid Voltage Dips’, IEEE Transactions on Power Electronics, 2017, 32, (11), pp. 8868-8879. doi: 10.1109/TPEL.2017.2648119

[22]Tsuneo, Y.: ‘Lyapunov Stability Theory’: ‘Foundations of Robotics: Analysis and Control’ (MITP, 2003), pp. 1

[23]Hu, S.S.: ‘Automatic Control Theory’ (Scientific Pubilisher, 2007.)

[24]Energinet, D.: ‘Technical regulation 3.2.2 for PV power plants above 11 kW’, in Editor: ‘Book Technical regulation 3.2.2 for PV power plants above 11 kW’ (Tech. Rep, 2015, edn.), pp.